IEEE Open Journal of
Antennas and Propagation

Received 22 July 2021; revised 9 November 2021; accepted 10 November 2021. Date of publication 15 November 2021; date of current version 24 November 2021.

Digital Object Identifier 10.1109/OJAP.2021.3128015

Ultra-Wideband Patch Antenna Array With an Inclined Proximity Coupled Feed for Small Unmanned Aircraft RADAR Applications

ABHISHEK K. AWASTHI[1] (Member, IEEE), CHRISTOPHER D. SIMPSON[2], SHRINIWAS KOLPUKE[2] (Graduate Student Member, IEEE), TUAN D. LUONG[2], JIE-BANG YAN[1] (Senior Member, IEEE), DREW TAYLOR[1] (Member, IEEE), AND S. PRASAD GOGINENI[2] (Life Fellow, IEEE)

[1]Department of Electrical and Computer Engineering, The University of Alabama, Tuscaloosa, AL 35487, USA

[2]Department of Aerospace Engineering and Mechanics, The University of Alabama, Tuscaloosa, AL 35487, USA

CORRESPONDING AUTHOR: A. K. AWASTHI (e-mail: aawasthi1@ua.edu)

This work was supported in part by the National Oceanic and Atmospheric Administration/University Corporation for Atmospheric Research (UCAR) under Contract NA18NWS4620043B.

ABSTRACT This paper presents the design of a lightweight and compact patch antenna array with an inclined proximity coupled feed. The antenna array is designed for operation on a small unmanned aircraft system (sUAS) with an ultra-wideband (UWB) radar for remote sensing of soil moisture and snow. To achieve UWB impedance matching, the design utilizes an inclined wide feed and inter-element coupling. A 3-D printed base (polylactic acid) is used to support the feed structure. The antenna array operates over a 2.5 GHz – 4.5 GHz frequency (57.2% bandwidth) range, and its weight is 112 grams. A prototype 2 × 4 element array is fabricated and tested. The antenna array has an 88.2% average radiation efficiency and a 13.2 dBi average realized gain over the desired frequency band with broadside and stable radiation pattern.

INDEX TERMS Patch antenna array, inter-element coupling, wideband, L-probe feed, radar.

I. INTRODUCTION

SMALL unmanned aircraft system (sUAS)-based radars have been developed and used for Earth remote sensing applications in recent years [1]–[2]. sUAS-based radars must be lightweight and compact due to the payload weight and size limitations. The antenna array, as a subsystem of the radar, also needs to be compact and lightweight. A few studies have reported the development of lightweight and compact antenna arrays for a sUAS [3]–[7]. For instance, Burr *et al.* developed a planar log-periodic dipole antenna array (63 grams) and TEM horn with a 3-D printed base (178 grams) for UAV radars [5]; Hilliard *et al.* presented a lightweight wing antenna array (122 grams) for small UAV radiometer applications [6]; and Lampersberger *et al.* [7] and Midtbøen *et al.* [8] fabricated lightweight horn antennas with 3-D printing techniques for UAVs.

High-gain antennas with narrow beamwidths are required to achieve fine angular resolution and high radar sensitivity. Patch antennas are inherently the first choice for these applications due to their low-profile and lightweight. The small impedance bandwidth of a patch antenna, however, limits its application, especially for use with ultra-wideband radars [9]. Several studies employ methods such as the U-slot patch and proximity coupled feed to achieve bandwidth enhancement of patch antennas. Pozar and Kaufman reported wideband microstrip patch antennas with a proximity coupled feed that achieved a 13% impedance bandwidth [10]. Mak *et al.* designed a patch antenna combining the U-slot and proximity coupled feed, which achieved a 20% impedance bandwidth and 7.5 dBi average gain [11]. Lau *et al.* used a wideband U-slot patch with a π-shaped aperture coupled feed and achieved a 27% impedance bandwidth and 13 dBi average gain [12]. Lo *et al.* reported a four-element patch antenna array for a communication system with an L-probe feed with a 22.2% impedance bandwidth [13]. Wong and Luk developed a folded patch with an L-probe feed to achieve both a wide band (20% bandwidth) and a wide beamwidth (103°) [14]. Qi *et al.* used a tilted L-probe feed for bandwidth enhancement and achieved a 37.1% bandwidth and 7.93 dBi average gain [15].

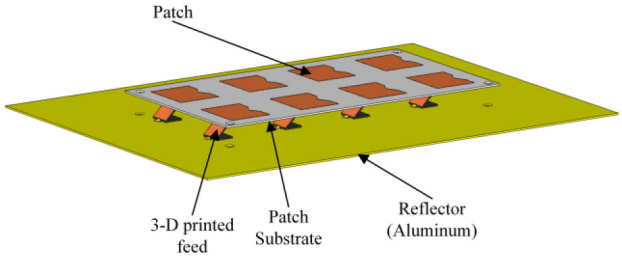

FIGURE 1. Geometry of the proposed antenna array.

Wang *et al.* designed and reported a single-layer U-slot patch antenna array with an 18.1% bandwidth and 11.5 dBi gain [16]. Awasthi *et al.* developed a wideband U-slot patch antenna array at 243.75 MHz over a bandwidth of 62.5% with a modified U-shaped feed for airborne wideband radar applications [17]. However, this structure is very heavy and not suitable for lightweight applications because it was developed for a long-range aircraft. Although several techniques have been proposed for the bandwidth enhancement of patch antennas, a bandwidth greater than 50% is difficult to achieve with a compact lightweight structure. Herscovici proposed a novel patch antenna design with an inclined probe feed [18]; this antenna has a very wide impedance bandwidth, but its radiation bandwidth is limited to 40%.

This paper presents the design and development of a wideband lightweight patch antenna array for sUAS-based radar applications. Ultra-wideband performance is achieved by using an electrically thick air substrate, inclined 3-D printed feed, and inter-element coupling. The proposed antenna array exhibits an active reflection coefficient below −10 dB over a 2.5-4.5 GHz frequency range. The antenna array has a 13.2 dBi average realized gain over the frequency of operation. The total size of the array is 240 mm × 160 mm × 22 mm. The antenna array with SMA connectors weighs only 112 grams. Section II discusses antenna design, Section III provides measurements results including fabrication issues, and Section IV discusses integration of the arrays into the UWB radar.

II. ANTENNA ARRAY DESIGN

Fig. 1 shows the geometry of the antenna array with printed patches on a dielectric substrate with no ground plane. The dielectric substrate is mounted over an aluminum plate that serves as the ground, so in the proposed array design patches are suspended on a thick air layer. Microstrip patch antennas with thick substrate and low dielectric constant exhibit broadband performance [19]. A thick air layer in the antenna array serves as thick substrate in this design. Fig. 2 shows the dimensions of the proposed antenna array, where the size of the reflector is L_g *mm* × W_g *mm*. Patches with dimensions of L_p *mm* × W_p *mm* are printed on a *240 mm* × *160 mm* (L_s × W_s) *Rogers RO4350* substrate with a thickness of *30 mil* and relative dielectric constant of *3.66*. The spacing between the elements is *40 mm* in the *x*- and *y*-directions. Fig. 2(b) shows the assembly of the feed structure, reflector, and patch substrate. The reflector and patch substrate are placed over the feed structure using nylon spacers. This arrangement eases the fabrication process and makes the structure mechanically stable for sUAS applications. The antenna array is simulated using *CST Microwave Studio*.

A. MODIFIED FEED DESIGN

Fig. 2(c) shows a detailed view of the modified feed structure. The feed is a modified L-probe proximity coupled feed. A wide copper strip is used instead of a thin rod [13]–[14] and is inclined at an angle of 45°. The base of feed is 3-D printed and copper tape is used for the electrical connections. Fig. 2(c) illustrates how the feed structure is connected to the inner pin of the SMA connector. The upper flat section of the feed is proximity-coupled to the patch through the dielectric substrate. The overall height of the feed is *10 mm*.

Fig. 3(a) shows the evolution of the feed structure. The initial design (Feed 1) is a conventional narrow strip width L-probe feed. This design is further modified in Feed 2 as a wide strip width L-probe feed to improve the active reflection coefficient in a finite array environment. The final structure is a wide-strip inclined feed. Fig. 3(b) shows the active reflection coefficient [20] for the three feed structures. Due to the symmetry of the array, only the results for four elements are shown. The center elements (3 and 4) are better matched to 50 ohms than the outer elements (1 and 2) because of the high inter-element coupling. The wide-strip inclined feed provided a significant improvement in the active reflection coefficient.

Fig. 4(a) shows the active reflection coefficient of elements 1 and 3 for various feed widths (w_f) obtained while holding the remaining parameters constant. In these results, feed width variation significantly affects the active reflection coefficient. For a wider feed width, the impedance match improves over a wide frequency range. The use of a wider strip provides higher capacitive coupling between the patch and the feed. This capacitive coupling compensates for the probe inductance of the electrically thick patch antenna. However, for a large feed width, the active reflection coefficient of the outer elements starts to degrade. This phenomenon imposes an upper limit on the value of the feed width. The active reflection coefficients of elements 1 and 3 for different values of the length of the flat section of feed (l_f) are shown in Fig. 4(b). A −10 dB active reflection coefficient bandwidth and in-band matching are both affected by the variation in l_f.

Fig. 5(a) shows the active reflection coefficient variation with respect to the feed angle. For a vertical feed (an angle of 90°), the match is poor, but it improves by decreasing the feed angle. For a 45° feed angle, the antenna array exhibits an active reflection coefficient below −10 dB for elements 1 and 3 over 2.5-4.5 GHz.

B. INTER-ELEMENT COUPLING

Inter-element coupling has a significant effect on the performance of the proposed antenna array. Fig. 5(b) shows a comparison of the single-element reflection coefficient and the active reflection coefficient of the antenna array. The

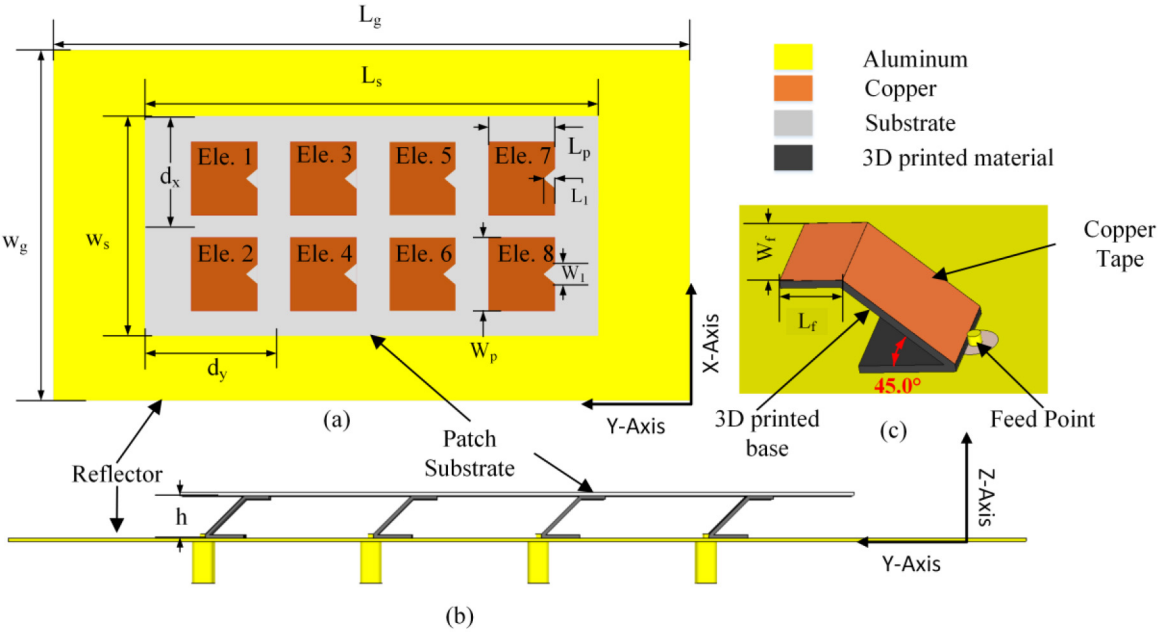

FIGURE 2. Various dimensions of the proposed antenna array (a) top view, (b) side view and (c) detailed feed structure. $L_g = 240$, $W_g = 160$, $L_p = 24.3$, $W_P = 22$, $L_s = 160$, $W_s = 80$, $L_1 = 3.5$, $W_1 = 10.4$, $h = 10$, $L_f = 6$, $W_f = 10$, $d_x = 40$, and $d_y = 40$. All dimensions are in mm.

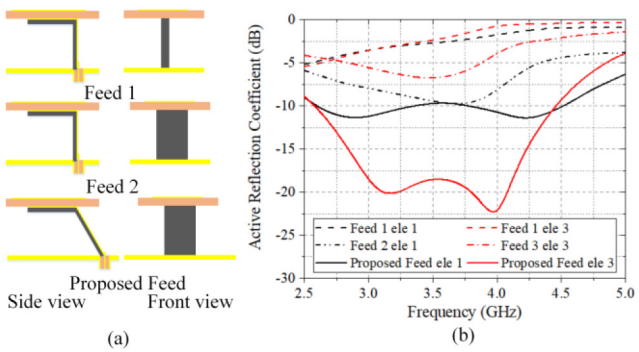

FIGURE 3. Modified feed evolution (a) evolution of the feed structure and (b) active reflection coefficient comparison for different feeds.

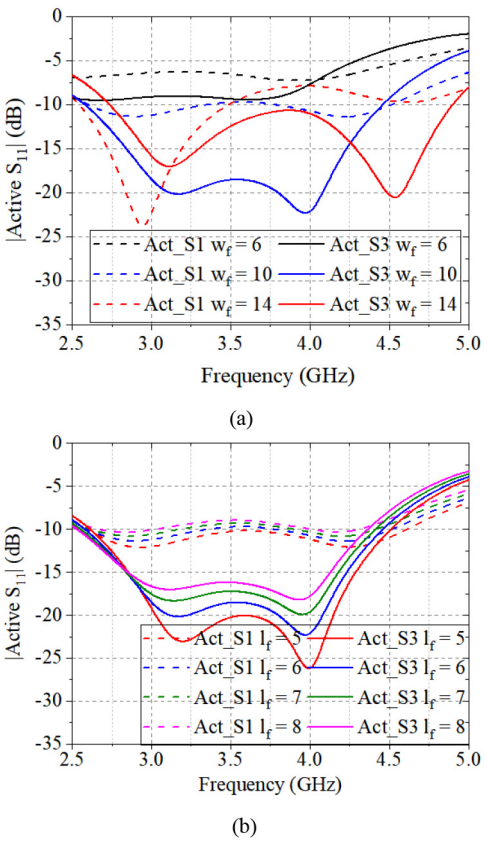

FIGURE 4. Active reflection coefficient variation for (a) feed width W_f and (b) feed length L_f.

single-element reflection coefficient is obtained by exciting element 1 alone and terminating the rest of the elements with matched loads. The active reflection coefficient is obtained by exciting all array elements simultaneously. Therefore, the active reflection coefficient accounts for the inter-element coupling in the antenna array. The simulation results show that the input impedance match is improved significantly in the case of the active reflection coefficient. Additionally, for the center element (element 3), the input impedance match is better than that of the outer element (element 1) due to the higher inter-element coupling. The array has only eight elements with each element experiencing a different coupling environment. Fig. 6 shows the magnitude of the *S-parameters* of elements 1 and 3. Corresponding *S-parameters* are obtained by exciting one element (element 1 or element 3) and terminating other elements in a matched load. In the case of the excitation of element 1, both elements 2 and 3 provide high mutual coupling, while in the case of the excitation of element 3, high mutual coupling is

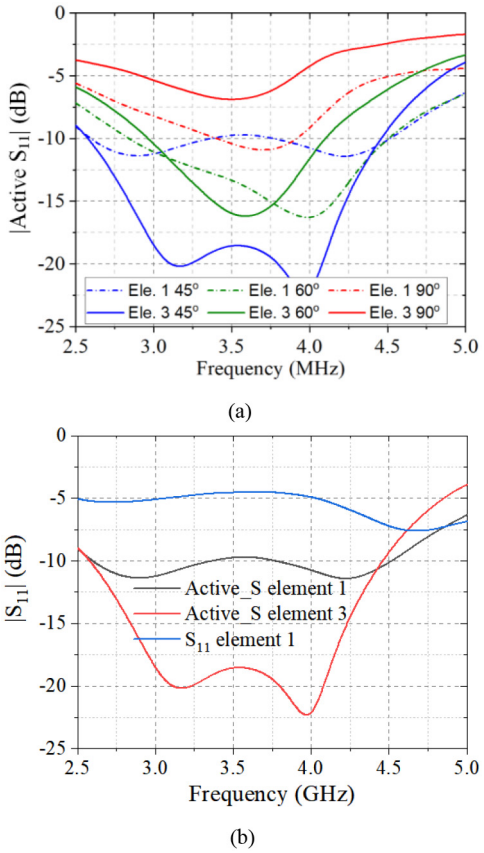

FIGURE 5. (a) Active reflection coefficient variation for different feed angles and (b) comparison of the reflection coefficient (single element excited) and the active reflection coefficient (all elements excited simultaneously) of the antenna array.

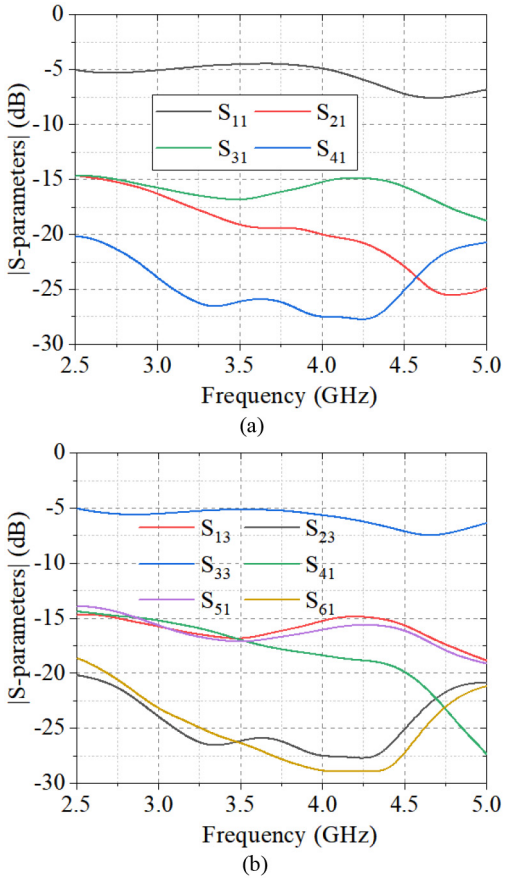

FIGURE 6. Reflection coefficient and coupling with close elements for (a) element 1 and (b) element 3.

provided by elements 1, 4 and 5, indicating that the center elements are experiencing higher inter-element coupling as compared to the edge elements. Therefore, different parameters of the antenna array can be optimized with a full finite array simulation.

This approach is different than the traditional antenna array design, wherein the single element is optimized in a free space environment and used as an array element for the full design. The above approach assumes that the mutual coupling among elements of the array is very small and does not affect the input impedance match of a single element in the array environment. For a small finite array, coupling between elements varies and depends on the geometry of the structure. Therefore, a similar active reflection coefficient response is difficult to achieve for all array elements. The design goal for a small finite array with high inter-element coupling is to obtain a -10 dB active reflection coefficient for all elements over the frequency of operation.

Fig. 7 shows the effect of inter-element spacing on the antenna array performance. Fig. 7(a) shows the active reflection coefficient for different values of separation, d_x, between elements in the x-direction, and Fig. 7(b) shows the active reflection coefficient for different values of separation, d_y, in the y-direction. The inter-element coupling decreases with increasing separation between elements. The spacing has a much stronger effect on the center elements than on the outer elements and influences only the mid-frequency band impedance match for the outer elements. The lower limit of the element spacing is identified for the optimum mid-frequency band impedance match for the edge elements. Standard patch antenna design equations are used to determine the patch antenna dimensions and optimized further through EM simulations to enhance the impedance bandwidth and maximize the realized gain of the antenna array.

III. FABRICATION AND MEASURED RESULTS

The antenna array is fabricated and tested it to verify the simulation results. Fig. 8(a) shows the fabricated prototype of the antenna array. Using a vector network analyzer, the reflection coefficient of each element and the mutual coupling between two elements of the antenna array are measured by terminating the remaining elements with 50-ohm loads.

The complete S-parameter matrix of 8×8 elements is measured to compute the active reflection coefficient. The active reflection coefficients of the antenna array are computed from the measured S-parameter matrix using equation (1),

$$\{S_{\text{Active}}\} = [S]\{V_i\} \tag{1}$$

where S_{Active} is the active reflection coefficient, $[S]$ is the measured S-parameter matrix, and $\{V_i\}$ is a vector of ones for

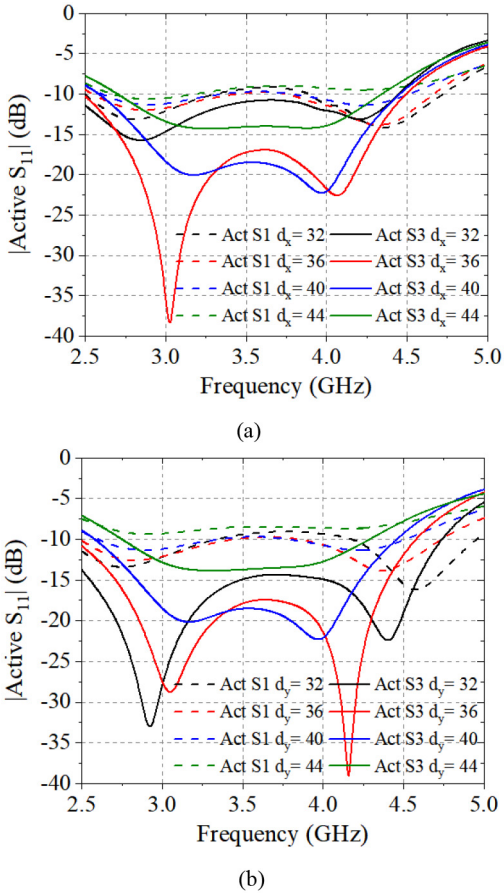

FIGURE 7. Active reflection coefficient variation for element spacing (a) in the *x-direction* d_X and (b) in the *y-direction* d_Y.

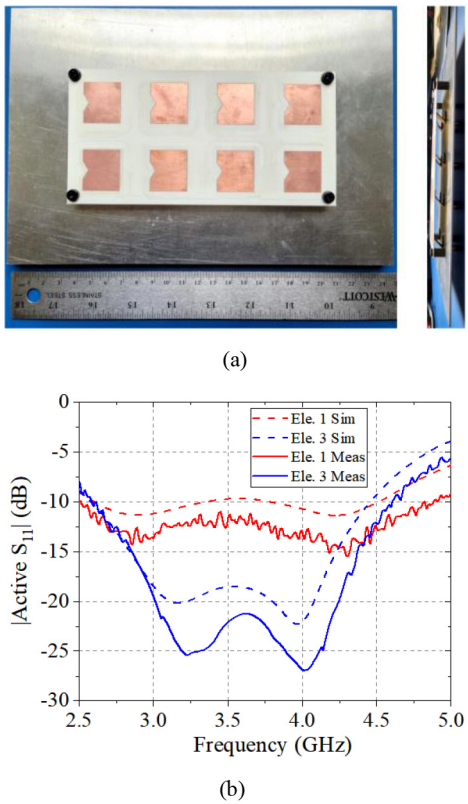

FIGURE 8. (a) Fabricated antenna array: top view and side view, (b) measured and simulated active S_{11}.

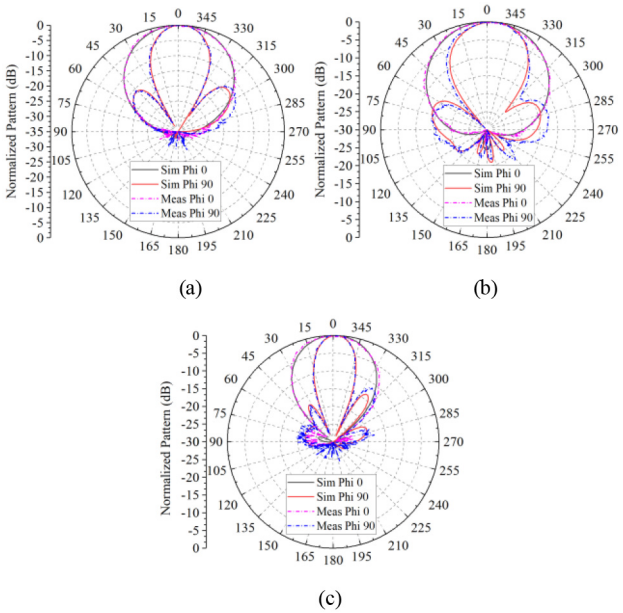

FIGURE 9. Measured and simulated radiation patterns of the antenna array: (a) 2.5 GHz, (b) 3.5 GHz and (c) 4.5 GHz.

uniform excitations. The magnitude of computed and simulated active S_{11} of the antenna array are plotted in Fig. 7(b). Only the results for elements 1 and 3 are shown here due to symmetry in the antenna structure. The computed and measured results match within 5 dB. The mismatch in the results is mainly due to errors in the phase measurement of the *S-parameters*. Phase errors from each *S-parameter* measurement are summed in the computation of the active reflection coefficient. In some cases, the net error is cancelled out due to the vector sum, and the results showed a very good match with the simulated results. In other cases, the cumulative error increased due to the vector sum.

The radiation patterns of the antenna array are measured using a 1 : 8 power divider. The measured and simulated radiation patterns of the proposed antenna array at different frequencies are shown in Fig. 9. The radiation pattern of the array is very stable in both the phi = 0° and phi = 90° planes. The measured and simulated results have some mismatch in the side lobe levels, which is mainly due to error in the measurement setup and power divider phase imbalance. Fig. 10 shows the total efficiency and realized gain as a function of the frequency. The efficiency is more than 85% above the frequency band of operation. The realized gain is 9.4 dBi at 2.5 GHz, and the maximum gain is 15 dBi at 4.25 GHz. The measured efficiency is calculated from the measured 3D radiation pattern of the antenna array [21] by taking the ratio of the integrated radiated power with the input power to the antenna array. The results showed

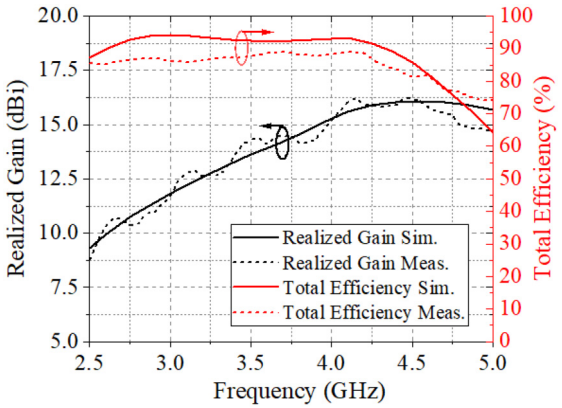

FIGURE 10. Realized gain and total efficiency of the antenna array.

TABLE 1. Comparison of proposed array with published research.

Ref.	BW (%)	Frequency band	Ave. Gain dBi	–
[12]	27 (SWR < 2)	3.4 GHz-4.5 GHz	13	2×2 array
[13]	22.2 (SWR < 1.5)	1550 MHz – 1950 MHz	--	1×4 array
[14]	20 (SWR < 1.5)	824 MHz-960 MHz	--	1×2 array
[15]	37.1(SWR < 2)	3.42 GHz- 4.98 GHz	7.93	Single element
[16]	18.1 (SWR<2)	5.65 GHz-6.78 GHz	11.5	2×2 array
This paper	57.2 (SWR < 2)	2.5 GHz-4.5 GHz	13.2	2×4 array

very good match between the measured and simulated realized gain and efficiency. Table 1 shows a comparison of the performance of the proposed array with other published research. The realized gain of the antenna array increases with frequency, and the power received by a radar is directly proportional to the product of antenna gain and square of the wavelength [22]. If gain is kept constant, the received power will decrease with frequency. This is not a desirable radar attribute. For radar backscatter measurements from the distributed target, increasing antenna gain with frequency is more suitable than providing a constant antenna gain over the frequency range of operation.

IV. RADAR SYSTEM INTEGRATION AND FIELD TEST

Field data collected during test flights at the University of Alabama Arboretum provide a means to verify the performance of the antenna array with a radar system. An FM-CW radar operating over the frequency range of 2.5-6.5 GHz with these antenna arrays is integrated with an Xfold Dragon X6 multirotor sUAS drone A detailed description of the radar is available in Simpson *et al.* [24]. Table 2 provides a summary of the radar parameters. In the current radar system design, the antenna sub-system consists of two antenna arrays, two 1 : 8 power dividers, and 16 coaxial cables. The total weight of the antenna sub-system including the power divider and cables is 740 grams.

TABLE 2. Radar parameter summary.

Parameter	Value	Unit
Frequency Band	2.5-6.5	GHz
Pulse Repetition Interval	2.5	ms
Pulse Duration	2	ms
Antenna Gain (2-way, at 3GHz)	23.6	dBi
Incident angle	20	Degree
Transmit Power	16.7	dBm
Receiver gain	~35	dB
Noise Figure (receiver)	3	dB
Path loss (2-way,100 meter altitude)	86.4	dB
Total weight	11	Lbs

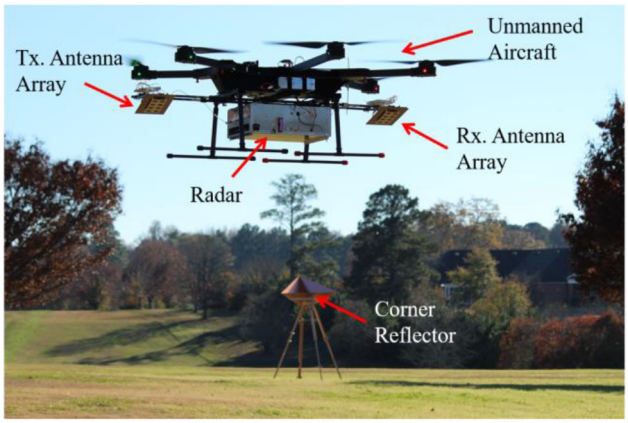

(a)

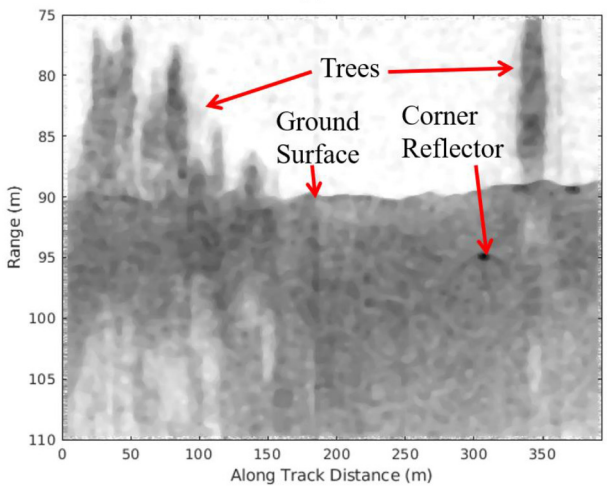

(b)

FIGURE 11. Field Test (a) Assembly of the radar system and antenna array, with the sUAS and (b) echogram generated from the processed field data.

Fig. 11(a) shows a photograph of the sUAS with the integrated radar and antenna during one of the flight tests. The

radar is suspended beneath the sUAS, as shown in the image. The transmit (Tx) and receive (Rx) antenna arrays are connected to the radar transmitter and receiver with short cables, respectively. The Tx and Rx antenna arrays are mounted 1.5 m apart to obtain the high isolation (>50 dB) required between the transmitter and receiver of the FM-CW radar. The arrays are mounted on the sUAS to illuminate the surface at a 20° incidence angle. The sUAS was flown at 100 m altitude above the starting elevation, and a constant altitude was maintained relative to mean sea level for the duration of the flight. The terrain elevation varies by less than 10 m over the measurement site. From this altitude the Tx and Rx antenna array footprints overlap. Hence, the radar system operates as a monostatic FM-CW radar with separate Tx and Rx antennas. The corner reflector shown in Fig. 11(a) is used to calibrate the radar data for backscatter measurements during field tests. The radar system also includes a GPS-INS receiver for determining the sUAS trajectory for synthetic aperture radar (SAR) processing and geolocation of the radar data. A remote-controlled relay enables the pilot to power the transmitter once the sUAS reaches its nominal flight altitude of 100 m to prevent close-range reflections from damaging the transmitter and receiver. The grid of the flight lines is defined first to cover a variety of terrains and vegetation profiles. Some of the flights also cover small water bodies (ponds). Measurements are carried out to collect the backscattered signal from the entire grid.

The backscattered signal from the trees and surface collected by receive antenna-array is amplified, digitized, and saved to on-board storage for further processing on the ground. A MATLAB-based SAR [24] algorithm is developed for the further processing of the collected field data. Fig. 11(b) shows sample results obtained over a flight line. These data are processed with an unfocussed SAR algorithm to generate a quick-look image. The unfocussed SAR algorithm consisted of coherently integrating data over an unfocussed aperture of length ($L = 1.2\sqrt{R\lambda}$, where R is the range of the radar target) and incoherently averaging 4 samples to reduce speckle in the along-track direction. The flight line shown in Fig. 11(b) includes areas with 2-15 m tall trees, short grass, and bare soil. Backscatter from the tree canopy and the surface below the trees are mapped by the radar. Future work includes more advanced processing to generate fully focused SAR images of calibrated backscatter data. The backscatter data with in-situ soil moisture measurements and vegetation characteristics can be used to estimate soil moisture and vegetation biomass over the measurement area.

V. CONCLUSION

The research team developed an ultra-wideband lightweight patch antenna array with a modified proximity feed and inter-element coupling to enhance the impedance bandwidth of the antenna array. The antenna array operates over the frequency band of 2.5 GHz – 4.5 GHz with a peak gain of 15 dBi, and the radiation pattern is very stable over the desired band of operation. Overall, the measured results agree very well with the simulated results. The antenna array performance is also verified with radar and sUAS.

REFERENCES

[1] T. Niedzielski *et al.*, "Estimating snow water equivalent using unmanned aerial vehicles for determining snow-melt runoff," *J. Hydrol.*, vol. 578, pp. 1–10, Nov. 2019.
[2] K. Wu *et al.*, "A new drone-borne GPR for soil moisture mapping," *Remote Sens. Environ.*, vol. 235, pp. 1–9, Dec. 2019.
[3] A. N. M. Kumari, S. Varughese, and P. V. Rao, "Miniaturized ultra-wideband printed dipole array for electronic warfare applications in unmaanned aerial vehicle systems," *Microw. Opt. Technol. Lett.*, vol. 62, no. 11, pp. 3601–3610, 2020.
[4] L. Scorrano, A. Manna, D. Spaziani, F. Trotta, P. Naglieri, and M. Ferrari, "A novel ultra-wideband UHF low-profile monopole for UAV platforms," in *Proc. Int. Symp. Antennas Propag. (ISAP)*, 2015, pp. 1–3.
[5] R. Burr, M. Schartel, W. Mayer, T. Walter, and C. Waldschmidt, "Lightweight broadband antennas for UAV based GPR sensors," in *Proc. 15th Eur. Radar Conf. (EuRAD)*, 2018, pp. 245–248.
[6] L. M. Hilliard, J. Mead, R. Rincon, and P. H. Hildebrand, "Lightweight linear broadband antennas enabling small UAV wing systems and space flight nanosat concept," in *Proc. Int. Geosci. Remote Sens. Symp.*, Anchorage, AK, USA, 2004, pp. 3577–3580.
[7] T. Lampersberger, R. Feger, A. Haderer, C. Egger, M. Friedl, and A. Stelzer, "A 24-GHz radar with 3D-printed and metallized lightweight antennas for UAV applications," in *Proc. 15th Eur. Radar Conf. (EuRAD)*, 2018, pp. 393–396.
[8] V. Midtbøen, K. G. Kjelgård, and T. S. Lande, "3D printed horn antenna with PCB microstrip feed for UWB radar applications," in *Proc. IEEE MTT-S Int. Microw. Workshop Series Adv. Mater. Processes RF THz Appl. (IMWS-AMP)*, 2017, pp. 1–3.
[9] S. Gogineni *et al.*, "Ultra-wideband radars for measurements over ICE and SNOW," in *Proc. IEEE Int. Geosci. Remote Sens. Symp. (IGARSS)*, 2015, pp. 4204–4207.
[10] D. M. Pozar and B. Kaufman, "Increasing the bandwidth of a microstrip antenna by proximity coupling," *Electron. Lett.*, vol. 23, no. 8, pp. 368–369, 1987.
[11] C. L. Mak, K. M. Luk, and K. F. Lee, "Proximity-coupled U-slot patch antenna," *Electron. Lett.*, vol. 34, no. 8, pp. 715–716, 1998.
[12] K. L. Lau, K. M. Luk, and K. F. Lee, "Wideband U-slot microstrip patch antenna array," *IEE Proc. Microw. Antennas Propag.*, vol. 148, no. 1, pp. 41–44, 2001.
[13] W. K. Lo, K. M. Shum, C. H. Chan, and K. M. Luk, "Wideband L-probe-fed base-station antenna array for PCS communication," in *Proc. Int. Symp. IEEE Antennas Propag. Soc.*, San Antonio, TX, USA, 2002, pp. 200–203.
[14] T. P. Wong and K. M. Luk, "A wideband L-probe patch antenna array with wide beamwidth," *IEEE Trans. Antennas Propag*. vol. 51, no. 10, pp. 3012–3014, Oct. 2003.
[15] D. Qi, B. Li, and H. Liu, "Wideband microstrip patch antenna with tilted L-probe feeding," *Microw. Opt. Technol. Lett*, vol. 43, no. 5, pp. 380–382, 2004.
[16] H. Wang, X. B. Huang, and D. G. Fang, "A single layer wide-band U-slot microstrip patch antenna array," *IEEE Antennas Wireless Propag. Lett.*, vol. 7, pp. 9–12, 2008
[17] A. K. Awasthi, J.-B. Yan, R. Hale, A. R. Harish, and S. P. Gogineni, "A modified feed U-slot patch antenna array for airborne very high frequency ice-penetrating radar," *Microw. Opt. Technol. Lett*. vol. 62, no. 1, pp. 378–386, 2020.
[18] N. Herscovici, "A wide-band single-layer patch antenna," *IEEE Trans. Antennas Propag.*, vol. 46, no. 4, pp. 471–474, Apr. 1998.
[19] D. M. Pozar, "Microstrip antennas," *Proc. IEEE*, vol. 80, no. 1, pp. 79–91, Jan. 1992.
[20] *IEEE Standard for Definitions of Terms for Antennas*, IEEE Standard 145-2013 (Revision of IEEE Std 145-1993), Mar. 2014.
[21] M. D. Foegelle. "Antenna Pattern Measurement: Concepts and Techniques." [Online]. Available: https://www.ets-lindgren.com/WhitePapers/APM.pdf (Accessed: Nov. 5, 2021).
[22] M. I. Skolnik, *Introduction to Radar Systems*. New York, NY, USA: McGraw-Hill, 2001.

[23] C. D. Simpson *et al.*, "Development of a UAS-based ultra-wideband radar for fine-resolution soil moisture measurements," in *Proc. IEEE Radar Conf. (RadarConf)*, Atlanta, GA, USA, 2021, pp. 1–4.
[24] M. Richard, *Fundamentals of Radar Signal Processing*, 2nd ed. Chicago, IL, USA: Tata McGraw-Hill Educ., 2005.

ABHISHEK K. AWASTHI (Member, IEEE) received the B.Tech. degree in electronics and communication engineering from Ajay Kumar Garg Engineering College Ghaziabad (UPTU Lucknow) in 2008, the M.Tech. degree in digital communication from the Ambedkar Institute of Technology Delhi (GGSIP University Delhi) in 2011, and the Doctoral degree from the Department of Electrical Engineering (RF and Microwave), Indian Institute of Technology Kanpur in 2018.

He served with the Department of Electronics Engineering, Madhav Institute of Technology & Science, Gwalior, as an Assistant Professor in 2018. After that, he joined the Electronics and Communication Department, Amity University Jharkhand. He is currently an Assistant Research Engineer with the Remote Sensing Center, The University of Alabama, Tuscaloosa, AL, USA. His current research interests include the design and analysis of antennas, phased antenna arrays, and ultrawideband radar systems.

CHRISTOPHER D. SIMPSON received the B.S. degree in aeronautics and astronautics engineering from Purdue University, West Lafayette, IN, USA, in 2010, and the M.S. degree in aerospace engineering and mechanics from The University of Alabama, Tuscaloosa, IN, USA, in 2016, where he is currently pursuing the Ph.D. degree in aerospace engineering and mechanics.

In Summer 2015, he interned with NASA Langley Research Center in Hampton, VA, USA. Since 2017, he has been a Graduate Research Assistant with the Remote Sensing Center, The University of Alabama. His research interests include the integration of remote sensing radar payloads into unmanned aircraft.

Mr. Simpson was a recipient of the Graduate Council Fellowship from The University of Alabama.

SHRINIWAS KOLPUKE (Member, IEEE) received the Bachelor of Engineering degree in electronics engineering from Swami Ramanand Teerth Marathwada University Nanded, India, in 2011, and the Master of Science in VLSI and embedded system design from Jawaharlal Nehru Technological University Hyderabad, India, in 2013. He is currently pursuing the Ph.D. degree with the Aerospace Engineering and Mechanics Department and works with the Remote Sensing Center, The University of Alabama, Tuscaloosa. He is currently pursuing research in the design, development, and optimization of FMCW radars for snow measurements towards his doctoral dissertation. After working in the industry for a brief time, he joined the Master of Science Program in aerospace engineering with the University of Kansas, Lawrence, and graduated in early 2017.

TUAN D. LUONG is currently pursuing the B.S. degree in aeronautics and astronautics engineering with The University of Alabama, Tuscaloosa, AL, USA.

Since 2019, he has been an Undergraduate Research Assistant with the Remote Sensing Center, The University of Alabama. His research interests include the control of unmanned aerial vehicles and the integration of sensors on different platforms.

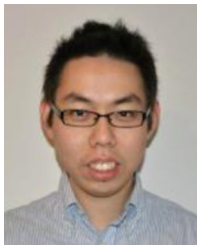

JIE-BANG YAN (Senior Member, IEEE) received the B.Eng. degree (First Class Hons.) in electronic and communications engineering from the University of Hong Kong, Hong Kong, in 2006, the M.Phil. degree in electronic and computer engineering from the Hong Kong University of Science and Technology, Hong Kong, in 2008, and the Ph.D. degree in electrical and computer engineering from the University of Illinois at Urbana-Champaign, Champaign, IL, USA, in 2011.

From 2009 to 2011, he was a Croucher Scholar with the University of Illinois at Urbana-Champaign, where he was involved in MIMO and reconfigurable antennas. In 2011, he joined the Center for Remote Sensing of Ice Sheets, University of Kansas, Lawrence, KS, USA, as an Assistant Research Professor. He is currently an Assistant Professor of Electrical and Computer Engineering and the Founding Deputy Director of the Remote Sensing Center, The University of Alabama, Tuscaloosa, AL, USA. He also has extensive airborne and ground-based radar deployment experience in both domestic and international regions, including Greenland and Antarctica. He holds two U.S. patents related to novel antenna technologies. His current research interests include the design and analysis of antennas and phased arrays, ultrawideband radar systems, radar signal processing, and remote sensing. He has received multiple research awards, including the Best Paper Award in the 2007 IEEE AP/MTT Postgraduate Conference, the UIUC Raj Mittra Outstanding Research Award in 2011, the NASA Group Achievement Award in 2013, the Best Paper Finalist of the 2015 National Instruments Week, the KU Leading Light Award in 2014, and the UA CoE Research and Innovation Award in 2019. He also serves as a Technical Reviewer for several journals and conferences on antennas and remote sensing.

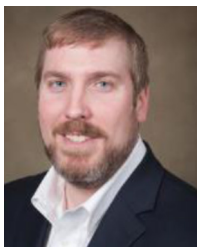

DREW TAYLOR (Member, IEEE) received the B.S. degree in electrical and computer engineering and M.S. degree in electrical engineering from The University of Alabama in 2008 and 2011, respectively, and the Ph.D. degree in electrical and computer engineering from Mississippi State University in 2018. Since this time, he has served as an Assistant Professor of Electrical and Computer Engineering with Remote Sensing Center, The University of Alabama. He serves as a technical reviewer for multiple journals and conferences across the fields of remote sensing and embedded systems.

S. PRASAD GOGINENI (Life Fellow, IEEE) is a Cudworth Professor of Engineering with The University of Alabama and the Director of the Remote Sensing Center. He was the founding Director of the NSF Science and Technology Center for Remote Sensing of Ice Sheets (CReSIS) with the University of Kansas from 2005 to 2016. He also led the development of ultrawideband radars for measuring the thickness of snow over sea ice and the mapping of internal layers in polar firn and ice. He has been involved with radar sounding and imaging of ice sheets for approximately 35 years and contributed to the first successful demonstration of SAR imaging of an ice bed through ice more than 3-km thick. He and his students developed early versions of radars being flown now as a part of the NASA OIB Mission. He received the Louise Byrd Graduate Educator Award at the University of Kansas and was a Fulbright Senior Scholar at the University of Tasmania in 2002. He is an IEEE Fellow and served as a Manager of NASA's Polar Program from 1997 to 1999.